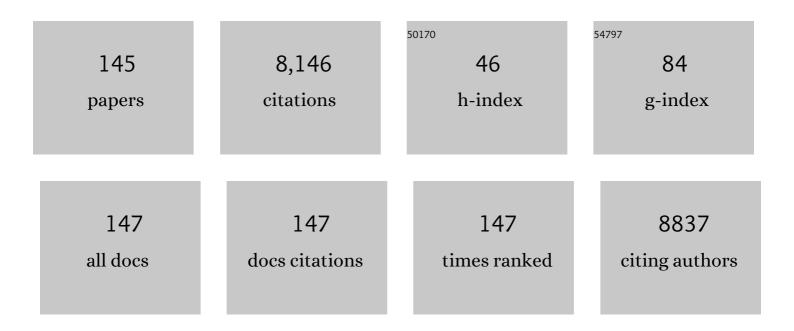


## List of Publications by Year in descending order

Source: https://exaly.com/author-pdf/4353764/publications.pdf Version: 2024-02-01



#	Article	IF	CITATIONS
1	Engineering surface oxygen vacancy of mesoporous CeO2 nanosheets assembled microspheres for boosting solar-driven photocatalytic performance. Chinese Chemical Letters, 2022, 33, 378-384.	4.8	32
2	Comparative study of metal oxides and phosphate modification with different mechanisms over g-C3N4 for visible-light photocatalytic degradation of metribuzin. Rare Metals, 2022, 41, 155-165.	3.6	50
3	Europium single atom based heterojunction photocatalysts with enhanced visible-light catalytic activity. Journal of Materials Chemistry A, 2022, 10, 5990-5997.	5.2	24
4	Valence-mixed iron phthalocyanines/(1 0 0) Bi2MoO6 nanosheet Z-scheme heterojunction catalysts for efficient visible-light degradation of 2-chlorophenol via preferential dechlorination. Chemical Engineering Journal, 2022, 440, 135786.	6.6	17
5	N-Rich Doped Anatase TiO2 with Smart Defect Engineering as Efficient Photocatalysts for Acetaldehyde Degradation. Nanomaterials, 2022, 12, 1564.	1.9	8
6	Synthesis of mixed-valence Cu phthalocyanine/graphene/g-C <sub>3</sub> N <sub>4</sub> ultrathin heterojunctions as efficient photocatalysts for CO <sub>2</sub> reduction. Catalysis Science and Technology, 2022, 12, 4817-4825.	2.1	6
7	Heterogeneous In/Mo cooperative bandgap engineering for promoting visible-light-driven CO <sub>2</sub> photoreduction. Journal of Materials Chemistry A, 2022, 10, 13393-13401.	5.2	8
8	Porous two-dimension MnO2-C3N4/titanium phosphate nanocomposites as efficient photocatalsyts for CO oxidation and mechanisms. Applied Catalysis B: Environmental, 2021, 282, 119563.	10.8	25
9	Dual functions of CO <sub>2</sub> molecular activation and 4f levels as electron transport bridges in erbium single atom composite photocatalysts therefore enhancing visible-light photoactivities. Journal of Materials Chemistry A, 2021, 9, 15820-15826.	5.2	26
10	Fabrication of N-CQDs@W18O49 heterojunction with enhanced charge separation and photocatalytic performance under full-spectrum light irradiation. Chinese Chemical Letters, 2021, 32, 3180-3184.	4.8	17
11	Recent advances in BiOBr-based photocatalysts for environmental remediation. Chinese Chemical Letters, 2021, 32, 3265-3276.	4.8	92
12	Erbium Single Atom Composite Photocatalysts for Reduction of CO <sub>2</sub> under Visible Light: CO <sub>2</sub> Molecular Activation and 4 <i>f</i> Levels as an Electron Transport Bridge. Small, 2021, 17, e2102089.	5.2	35
13	Controlled Synthesis of Nitro-Terminated Poly[2-(3-thienyl)-ethanol]/g-C <sub>3</sub> N <sub>4</sub> Nanosheet Heterojunctions for Efficient Visible-Light Photocatalytic Hydrogen Evolution. ACS Sustainable Chemistry and Engineering, 2021, 9, 7306-7317.	3.2	21
14	Dual Functions of CO <sub>2</sub> Molecular Activation and 4 <i>f</i> Levels as Electron Transport Bridge in Dysprosium Single Atom Composite Photocatalysts with Enhanced Visibleâ€Light Photoactivities. Advanced Functional Materials, 2021, 31, 2104976.	7.8	43
15	Surface defects induced charge imbalance for boosting charge separation and solar-driven photocatalytic hydrogen evolution. Journal of Colloid and Interface Science, 2021, 596, 12-21.	5.0	19
16	Energy Platform for Directed Charge Transfer in the Cascade Zâ€Scheme Heterojunction: CO <sub>2</sub> Photoreduction without a Cocatalyst. Angewandte Chemie, 2021, 133, 21074-21082.	1.6	23
17	Energy Platform for Directed Charge Transfer in the Cascade Zâ€Scheme Heterojunction: CO <sub>2</sub> Photoreduction without a Cocatalyst. Angewandte Chemie - International Edition, 2021, 60, 20906-20914.	7.2	132
18	Construction of Sixâ€Oxygenâ€Coordinated Single Ni Sites on gâ€C <sub>3</sub> N <sub>4</sub> with Boronâ€Oxo Species for Photocatalytic Waterâ€Activationâ€Induced CO <sub>2</sub> Reduction. Advanced Materials, 2021, 33, e2105482.	11.1	128

#	Article	IF	CITATIONS
19	Ultrathin phosphate-modulated zinc phthalocyanine/perylenete diimide supermolecule Z-scheme heterojunctions as efficiently wide visible-light photocatalysts for CO2 conversion. Chemical Engineering Journal, 2021, 426, 131266.	6.6	20
20	NiO nanoparticles dotted TiO2 nanosheets assembled nanotubes P-N heterojunctions for efficient interface charge separation and photocatalytic hydrogen evolution. Applied Surface Science, 2021, 568, 150981.	3.1	30
21	Efficiently photocatalytic degradation of monochlorophenol on in-situ fabricated BiPO4/β-Bi2O3 heterojunction microspheres and O2-free hole-induced selective dechloridation conversion with H2 evolution. Applied Catalysis B: Environmental, 2020, 263, 118313.	10.8	42
22	Enhanced Visibleâ€Light Photoactivities of Perovskiteâ€Type LaFeO <sub>3</sub> Nanocrystals by Simultaneously Doping Er <sup>3+</sup> and Coupling MgO for CO <sub>2</sub> Reduction. ChemCatChem, 2020, 12, 623-630.	1.8	14
23	Energy and separation optimization of photogenerated charge in BiVO4 quantum dots by piezo-potential for efficient gaseous pollutant degradation. Nano Energy, 2020, 69, 104448.	8.2	52
24	Construction of a triple sequential junction for efficient separation of photogenerated charges in photocatalysis. Chemical Communications, 2020, 56, 197-200.	2.2	11
25	Co-MOF as an electron donor for promoting visible-light photoactivities of g-C3N4 nanosheets for CO2 reduction. Chinese Journal of Catalysis, 2020, 41, 514-523.	6.9	72
26	Emerging layered BiO <sub>2â^'x</sub> for photocatalysis: status, challenges, and outlook. Sustainable Energy and Fuels, 2020, 4, 5378-5386.	2.5	19
27	Inhibition of Sn( <scp>ii</scp> ) oxidation in <i>Z</i> -scheme BiVO <sub>4</sub> -QD@Sn <sub>3</sub> O <sub>4</sub> for overall water splitting. Chemical Communications, 2020, 56, 13884-13887.	2.2	16
28	Efficient singlet oxygen generation by excitonic energy transfer on ultrathin g-C3N4 for selective photocatalytic oxidation of methyl-phenyl-sulfide with O2. Chinese Chemical Letters, 2020, 31, 2784-2788.	4.8	52
29	Efficiently photocatalytic conversion of CO2 on ultrathin metal phthalocyanine/g-C3N4 heterojunctions by promoting charge transfer and CO2 activation. Applied Catalysis B: Environmental, 2020, 277, 119199.	10.8	84
30	Highly sensitive fluorescence detection of chloride ion in aqueous solution with Ag-modified porous g-C3N4 nanosheets. Chinese Chemical Letters, 2020, 31, 2725-2729.	4.8	26
31	Ultrafine SnO <sub>2</sub> /010 Facet-Exposed BiVO <sub>4</sub> Nanocomposites as Efficient Photoanodes for Controllable Conversion of 2,4-Dichlorophenol via a Preferential Dechlorination Path. ACS Applied Materials & Interfaces, 2020, 12, 28264-28272.	4.0	19
32	Accelerated generation of hydroxyl radical through surface polarization on BiVO4 microtubes for efficient chlortetracycline degradation. Chemical Engineering Journal, 2020, 400, 125871.	6.6	49
33	Rareâ€Earth Single Erbium Atoms for Enhanced Photocatalytic CO <sub>2</sub> Reduction. Angewandte Chemie, 2020, 132, 10738-10744.	1.6	49
34	Rareâ€Earth Single Erbium Atoms for Enhanced Photocatalytic CO <sub>2</sub> Reduction. Angewandte Chemie - International Edition, 2020, 59, 10651-10657.	7.2	314
35	Synthesis of SnO2/yolk-shell LaFeO3 nanocomposites as efficient visible-light photocatalysts for 2,4-dichlorophenol degradation. Materials Research Bulletin, 2020, 127, 110857.	2.7	47
36	Mgâ^'Oâ€Bridged Polypyrrole/g <sub>3</sub> N <sub>4</sub> Nanocomposites as Efficient Visibleâ€Light Catalysts for Hydrogen Evolution. ChemSusChem, 2020, 13, 3707-3717.	3.6	19

#	Article	IF	CITATIONS
37	Ti <sub>2</sub> O <sub>3</sub> /TiO <sub>2</sub> heterophase junctions with enhanced charge separation and spatially separated active sites for photocatalytic CO <sub>2</sub> reduction. Physical Chemistry Chemical Physics, 2020, 22, 4526-4532.	1.3	44
38	Covalent-organic framework based Z-scheme heterostructured noble-metal-free photocatalysts for visible-light-driven hydrogen evolution. Journal of Materials Chemistry A, 2020, 8, 4334-4340.	5.2	85
39	The synthesis of interface-modulated ultrathin Ni( <scp>ii</scp> ) MOF/g-C <sub>3</sub> N <sub>4</sub> heterojunctions as efficient photocatalysts for CO <sub>2</sub> reduction. Nanoscale, 2020, 12, 10010-10018.	2.8	64
40	Recyclable adsorbent of BiFeO3/Carbon for purifying industrial dye wastewater via photocatalytic reproducible. Green Energy and Environment, 2019, 4, 66-74.	4.7	26
41	Innentitelbild: Dimensionâ€Matched Zinc Phthalocyanine/BiVO <sub>4</sub> Ultrathin Nanocomposites for CO <sub>2</sub> Reduction as Efficient Wideâ€Visibleâ€Lightâ€Driven Photocatalysts via a Cascade Charge Transfer (Angew. Chem. 32/2019). Angewandte Chemie, 2019, 131, 10878-10878.	1.6	0
42	Improved Photoactivities of Largeâ€surfaceâ€area gâ€C <sub>3</sub> N <sub>4</sub> for CO <sub>2</sub> Conversion by Controllably Introducing Coâ€and Niâ€Species to Effectively Modulate Photogenerated Charges. ChemCatChem, 2019, 11, 6282-6287.	1.8	15
43	Dimensionâ€Matched Zinc Phthalocyanine/BiVO <sub>4</sub> Ultrathin Nanocomposites for CO <sub>2</sub> Reduction as Efficient Wideâ€Visibleâ€Lightâ€Driven Photocatalysts via a Cascade Charge Transfer. Angewandte Chemie, 2019, 131, 10989-10994.	1.6	44
44	Surface co-modification with highly-dispersed Mn & Cu oxides of g-C3N4 nanosheets for efficiently photocatalytic reduction of CO2 to CO and CH4. Applied Surface Science, 2019, 492, 125-134.	3.1	51
45	Modulating the photoelectrons of g-C3N4 via coupling MgTi2O5 as appropriate platform for visible-light-driven photocatalytic solar energy conversion. Nano Research, 2019, 12, 1931-1936.	5.8	42
46	Dimensionâ€Matched Zinc Phthalocyanine/BiVO <sub>4</sub> Ultrathin Nanocomposites for CO <sub>2</sub> Reduction as Efficient Wideâ€Visibleâ€Lightâ€Driven Photocatalysts via a Cascade Charge Transfer. Angewandte Chemie - International Edition, 2019, 58, 10873-10878.	7.2	168
47	Improved visible-light photoactivities of porous LaFeO <sub>3</sub> by coupling with nanosized alkaline earth metal oxides and mechanism insight. Catalysis Science and Technology, 2019, 9, 3149-3157.	2.1	40
48	Promoted oxygen activation of layered micro-mesoporous structured titanium phosphate nanoplates by coupling nano-sized Î-MnO2 with surface pits for efficient photocatalytic oxidation of CO. Applied Catalysis B: Environmental, 2019, 254, 260-269.	10.8	33
49	Synthesis of activated carbon-supported TiO2-based nano-photocatalysts with well recycling for efficiently degrading high-concentration pollutants. Catalysis Today, 2019, 335, 557-564.	2.2	64
50	Synthesis of Si–O-Bridged <i>g</i> -C <sub>3</sub> N <sub>4</sub> /WO <sub>3</sub> 2D-Heterojunctional Nanocomposites as Efficient Photocatalysts for Aerobic Alcohol Oxidation and Mechanism Insight. ACS Sustainable Chemistry and Engineering, 2019, 7, 9916-9927.	3.2	44
51	Review of strategies for the fabrication of heterojunctional nanocomposites as efficient visible-light catalysts by modulating excited electrons with appropriate thermodynamic energy. Journal of Materials Chemistry A, 2019, 7, 10879-10897.	5.2	98
52	Luminescent material with functionalized graphitic carbon nitride as a photovoltaic booster in DSSCs: Enhanced charge separation and transfer. Journal of Materials Research, 2019, 34, 616-625.	1.2	7
53	Boosting the visible-light photoactivities of BiVO <sub>4</sub> nanoplates by Eu doping and coupling CeO <sub>x</sub> nanoparticles for CO <sub>2</sub> reduction and organic oxidation. Sustainable Energy and Fuels, 2019, 3, 3363-3369.	2.5	52
54	Synthesis of Au-decorated three-phase-mixed TiO <sub>2</sub> /phosphate modified active carbon nanocomposites as easily-recycled efficient photocatalysts for degrading high-concentration 2,4-DCP. RSC Advances, 2019, 9, 38414-38421.	1.7	9

#	Article	IF	CITATIONS
55	Improved photoelectric properties of BiOBr nanoplates by co-modifying SnO2 and Ag to promote photoelectrons trapped by adsorbed O2. Science China Materials, 2019, 62, 653-661.	3.5	9
56	Improved visible-light photoactivity of Pt/g-C3N4 nanosheets for solar fuel production via pretreated boric acid modification. Research on Chemical Intermediates, 2019, 45, 249-259.	1.3	16
57	Visible-light induced electron modulation to improve photoactivities of coral-like Bi2WO6 by coupling SnO2 as a proper energy platform. Catalysis Today, 2019, 327, 288-294.	2.2	11
58	Synthesis of ZnO/Bi-doped porous LaFeO3 nanocomposites as highly efficient nano-photocatalysts dependent on the enhanced utilization of visible-light-excited electrons. Applied Catalysis B: Environmental, 2018, 231, 23-33.	10.8	113
59	Promoting infrared light driven photocatalytic activity of W18O49 nanorods by coupling polypyrrole. Research on Chemical Intermediates, 2018, 44, 5455-5466.	1.3	7
60	Improved visible-light activities of nanocrystalline CdS by coupling with ultrafine NbN with lattice matching for hydrogen evolution. Sustainable Energy and Fuels, 2018, 2, 549-552.	2.5	35
61	Synthesis of Silicateâ€Bridged Heterojunctional SnO <sub>2</sub> /BiVO <sub>4</sub> Nanoplates as Efficient Photocatalysts to Convert CO <sub>2</sub> and Degrade 2,4â€Dichlorophenol. Particle and Particle Systems Characterization, 2018, 35, 1700320.	1.2	13
62	Synthesis of nano SnO2-coupled mesoporous molecular sieve titanium phosphate as a recyclable photocatalyst for efficient decomposition of 2,4-dichlorophenol. Nano Research, 2018, 11, 1612-1624.	5.8	37
63	Synthesis of Large Surfaceâ€Area gâ€C <sub>3</sub> N <sub>4</sub> Comodified with MnO <i><sub>x</sub></i> and Auâ€TiO <sub>2</sub> as Efficient Visibleâ€Light Photocatalysts for Fuel Production. Advanced Energy Materials, 2018, 8, 1701580.	10.2	157
64	Exceptional photocatalytic activities for CO2 conversion on Al O bridged g-C3N4/α-Fe2O3 z-scheme nanocomposites and mechanism insight with isotopesZ. Applied Catalysis B: Environmental, 2018, 221, 459-466.	10.8	154
65	Improved visible-light activities for degrading pollutants on TiO2/g-C3N4 nanocomposites by decorating SPR Au nanoparticles and 2,4-dichlorophenol decomposition path. Journal of Hazardous Materials, 2018, 342, 715-723.	6.5	190
66	One-dimension carbon self-doping g-C3N4 nanotubes: Synthesis and application in dye-sensitized solar cells. Nano Research, 2018, 11, 1322-1330.	5.8	35
67	Improved Visible-Light Activities of Rutile Nanorod by Comodifying Highly Dispersed Surface Plasmon Resonance Au Nanoparticles and HF Groups for Aerobic Selective Alcohol Oxidation. ACS Sustainable Chemistry and Engineering, 2018, 6, 14652-14659.	3.2	14
68	Dimension-matched plasmonic Au/TiO <sub>2</sub> /BiVO <sub>4</sub> nanocomposites as efficient wide-visible-light photocatalysts to convert CO <sub>2</sub> and mechanistic insights. Journal of Materials Chemistry A, 2018, 6, 11838-11845.	5.2	72
69	Exceptional visible-light activities of g-C3N4 nanosheets dependent on the unexpected synergistic effects of prolonging charge lifetime and catalyzing H2 evolution with H2O. Applied Catalysis B: Environmental, 2018, 237, 50-58.	10.8	51
70	BaWO <sub>4</sub> :Ln <sup>3+</sup> Nanocrystals: Controllable Synthesis, Theoretical Investigation on the Substitution Site, and Bright Upconversion Luminescence as a Sensor for Glucose Detection. ACS Applied Nano Materials, 2018, 1, 4762-4770.	2.4	14
71	A general strategy toward the large-scale synthesis of the noble metal-oxide nanocrystal hybrids with intimate interfacial contact for the catalytic reduction of p-nitrophenol and photocatalytic degradation of pollutants. Research on Chemical Intermediates, 2017, 43, 4759-4779.	1.3	4
72	Prolonged lifetime and enhanced separation of photogenerated charges of nanosized α-Fe2O3 by coupling SnO2 for efficient visible-light photocatalysis to convert CO2 and degrade acetaldehyde. Nano Research, 2017, 10, 2321-2331.	5.8	44

#	Article	IF	CITATIONS
73	Photogenerated electron modulation to dominantly induce efficient 2,4-dichlorophenol degradation on BiOBr nanoplates with different phosphate modification. Applied Catalysis B: Environmental, 2017, 209, 320-328.	10.8	91
74	Efficient photodecomposition of 2,4-dichlorophenol on recyclable phase-mixed hierarchically structured Bi <sub>2</sub> O <sub>3</sub> coupled with phosphate-bridged nano-SnO <sub>2</sub> . Environmental Science: Nano, 2017, 4, 1147-1154.	2.2	37
75	Enhanced photocatalytic activities of commercial P25 TiO 2 by trapping holes and transferring electrons for CO 2 conversion and 2,4-dichlorophenol degradation. Materials Research Bulletin, 2017, 92, 23-28.	2.7	21
76	Enhanced photoelectrochemical activities for water oxidation and phenol degradation on WO3 nanoplates by transferring electrons and trapping holes. Scientific Reports, 2017, 7, 1303.	1.6	23
77	Synthesis of TiO2/g-C3N4 nanocomposites with phosphate–oxygen functional bridges for improved photocatalytic activity. Chinese Journal of Catalysis, 2017, 38, 1072-1078.	6.9	45
78	Coordination and reduction in polyol-mediated solvothermal synthesis of nickel-based materials with controllable morphology and magnetic and electrochemical properties. Research on Chemical Intermediates, 2017, 43, 6395-6406.	1.3	5
79	Correlation of polypeptide N-acetylgalactosamine transferases-3 and -6 to different stages of endometriosis. Archives of Gynecology and Obstetrics, 2017, 295, 1413-1419.	0.8	4
80	Enhanced photoelectric conversion efficiency of dye-sensitized solar cells by the synergetic effect of NaYF4:Er3+/Yb3+ and g-C3N4. Science China Materials, 2017, 60, 228-238.	3.5	25
81	Down-shifting luminescence of water soluble NaYF4:Eu3+@Ag core-shell nanocrystals for fluorescence turn-on detection of glucose. Science China Materials, 2017, 60, 68-74.	3.5	22
82	Improved charge separation and surface activation via boron-doped layered polyhedron SrTiO3 for co-catalyst free photocatalytic CO2 conversion. Applied Catalysis B: Environmental, 2017, 219, 10-17.	10.8	113
83	MgTiO3/MgTi2O5/TiO2 heterogeneous belt-junctions with high photocatalytic hydrogen production activity. Nano Research, 2017, 10, 295-304.	5.8	20
84	Improved photoelectrocatalytic activities of BiOCl with high stability for water oxidation and MO degradation by coupling RGO and modifying phosphate groups to prolong carrier lifetime. Applied Catalysis B: Environmental, 2017, 203, 355-362.	10.8	107
85	Synthesis of SnO2/B-P codoped g-C3N4 nanocomposites as efficient cocatalyst-free visible-light photocatalysts for CO2 conversion and pollutant degradation. Applied Catalysis B: Environmental, 2017, 201, 486-494.	10.8	254
86	Coupling of Nanocrystalline Anatase TiO2 to Porous Nanosized LaFeO3 for Efficient Visible-Light Photocatalytic Degradation of Pollutants. Nanomaterials, 2016, 6, 22.	1.9	35
87	Visible-light-driven Fe2O3 nanoparticles/TiO2 array photoelectrode and its photoelectrochemical property. Research on Chemical Intermediates, 2016, 42, 7935-7946.	1.3	9
88	Synthesis of pure phase Mg1.2Ti1.8O5 and MgTiO3 nanocrystals for photocatalytic hydrogen production. Nano Research, 2016, 9, 726-734.	5.8	41
89	Co <sub>3</sub> O <sub>4</sub> nanosheets as a high-performance catalyst for oxygen evolution proceeding via a double two-electron process. Chemical Communications, 2016, 52, 6705-6708.	2.2	64
90	Large-scale synthesis of stable mesoporous black TiO <sub>2</sub> nanosheets for efficient solar-driven photocatalytic hydrogen evolution via an earth-abundant low-cost biotemplate. RSC Advances, 2016, 6, 50506-50512.	1.7	29

#	Article	IF	CITATIONS
91	Synthesis of hierarchical Mn 2 O 3 microspheres for photocatalytic hydrogen production. Materials Research Bulletin, 2016, 84, 99-104.	2.7	23
92	Exceptional Visibleâ€Lightâ€Driven Cocatalystâ€Free Photocatalytic Activity of gâ€C <sub>3</sub> N <sub>4</sub> by Well Designed Nanocomposites with Plasmonic Au and SnO <sub>2</sub> . Advanced Energy Materials, 2016, 6, 1601190.	10.2	207
93	Enhanced photoelectric conversion efficiency of dye sensitized solar cells via the incorporation of one dimensional luminescent BaWO <sub>4</sub> :Eu <sup>3+</sup> nanowires. Chemical Communications, 2016, 52, 11124-11126.	2.2	22
94	Exceptional Visible-Light Activities of TiO <sub>2</sub> -Coupled N-Doped Porous Perovskite LaFeO <sub>3</sub> for 2,4-Dichlorophenol Decomposition and CO <sub>2</sub> Conversion. Environmental Science & Technology, 2016, 50, 13600-13610.	4.6	146
95	Exceptional performance of photoelectrochemical water oxidation of single-crystal rutile TiO2 nanorods dependent on the hole trapping of modified chloride. Scientific Reports, 2016, 6, 21430.	1.6	30
96	Accepting Excited High-Energy-Level Electrons and Catalyzing H <sub>2</sub> Evolution of Dual-Functional Ag-TiO <sub>2</sub> Modifier for Promoting Visible-Light Photocatalytic Activities of Nanosized Oxides. Journal of Physical Chemistry C, 2016, 120, 11831-11836.	1.5	27
97	Enhanced Cocatalyst-Free Visible-Light Activities for Photocatalytic Fuel Production of g-C <sub>3</sub> N <sub>4</sub> by Trapping Holes and Transferring Electrons. Journal of Physical Chemistry C, 2016, 120, 98-107.	1.5	135
98	Enhanced charge separation of rutile TiO <sub>2</sub> nanorods by trapping holes and transferring electrons for efficient cocatalyst-free photocatalytic conversion of CO <sub>2</sub> to fuels. Chemical Communications, 2016, 52, 5027-5029.	2.2	45
99	Controlled synthesis of CaTiO <sub>3</sub> :Ln <sup>3+</sup> nanocrystals for luminescence and photocatalytic hydrogen production. RSC Advances, 2016, 6, 5761-5766.	1.7	22
100	Enhanced visible-light activities of porous BiFeO3 by coupling with nanocrystalline TiO2 and mechanism. Applied Catalysis B: Environmental, 2016, 180, 219-226.	10.8	223
101	Pure phase orthorhombic MgTi <sub>2</sub> O <sub>5</sub> photocatalyst for H <sub>2</sub> production. RSC Advances, 2015, 5, 106151-106155.	1.7	22
102	Synthesis of TiO2/g-C3N4 nanocomposites as efficient photocatalysts dependent on the enhanced photogenerated charge separation. Materials Research Bulletin, 2015, 70, 494-499.	2.7	75
103	Thin carbon layer coated Ti <sup>3+</sup> -TiO <sub>2</sub> nanocrystallites for visible-light driven photocatalysis. Nanoscale, 2015, 7, 5035-5045.	2.8	97
104	<i>In Situ</i> Carbon-Coated Yolk–Shell V <sub>2</sub> O <sub>3</sub> Microspheres for Lithium-Ion Batteries. ACS Applied Materials & Interfaces, 2015, 7, 1595-1601.	4.0	132
105	The promotion effect of surface negative electrostatic field on the photogenerated charge separation of BiVO <sub>4</sub> and its contribution to the enhanced PEC water oxidation. Chemical Communications, 2015, 51, 2821-2823.	2.2	42
106	A versatile salicylic acid precursor method for preparing titanate microspheres. Science China Materials, 2015, 58, 106-113.	3.5	6
107	ZnO-dotted porous ZnS cluster microspheres for high efficient, Pt-free photocatalytic hydrogen evolution. Scientific Reports, 2015, 5, 8858.	1.6	34
108	Enhanced visible-light activities for PEC water reduction of CuO nanoplates by coupling with anatase TiO2 and mechanism. Applied Surface Science, 2015, 351, 681-685.	3.1	25

#	Article	IF	CITATIONS
109	Synthesis of silicate-bridged ZnO/g-C <sub>3</sub> N <sub>4</sub> nanocomposites as efficient photocatalysts and its mechanism. RSC Advances, 2015, 5, 37275-37280.	1.7	40
110	Modification Strategies with Inorganic Acids for Efficient Photocatalysts by Promoting the Adsorption of O <sub>2</sub> . ACS Applied Materials & Interfaces, 2015, 7, 22727-22740.	4.0	68
111	Role of quaternary N in N-doped graphene–Fe <sub>2</sub> O <sub>3</sub> nanocomposites as efficient photocatalysts for CO <sub>2</sub> reduction and acetaldehyde degradation. RSC Advances, 2015, 5, 85061-85064.	1.7	27
112	Improved photoactivity of TiO <sub>2</sub> –Fe <sub>2</sub> O <sub>3</sub> nanocomposites for visible-light water splitting after phosphate bridging and its mechanism. Physical Chemistry Chemical Physics, 2015, 17, 5043-5050.	1.3	84
113	Synthesis of Ag–TiO2 Arrays Film for Photocatalytic Degradation of Dye and Water Splitting. Energy and Environment Focus, 2015, 4, 164-169.	0.3	4
114	Photocatalytic activity of MTiO <sub>3</sub> (M = Ca, Ni, and Zn) nanocrystals for water decomposition to hydrogen. Journal of Materials Research, 2014, 29, 1295-1301.	1.2	20
115	Hierarchical Nâ€Doped TiO <sub>2</sub> Microspheres with Exposed (001) Facets for Enhanced Visible Light Catalysis. European Journal of Inorganic Chemistry, 2014, 2014, 2146-2152.	1.0	29
116	Heterojunction Ag–TiO <sub>2</sub> Nanopillars for Visibleâ€Lightâ€Driven Photocatalytic H <sub>2</sub> Production. ChemPlusChem, 2014, 79, 995-1000.	1.3	15
117	Facile synthesis of stable magnetic fluid using size-controlled Fe3O4 nanoparticles. Materials Research Bulletin, 2014, 56, 34-38.	2.7	11
118	A floating macro/mesoporous crystalline anatase TiO <sub>2</sub> ceramic with enhanced photocatalytic performance for recalcitrant wastewater degradation. Dalton Transactions, 2014, 43, 790-798.	1.6	67
119	A New Combustion Route to Synthesize Mixed Valence Vanadium Oxide Heterojunction Composites as Visibleâ€Lightâ€Driven Photocatalysts. ChemCatChem, 2014, 6, 2553-2559.	1.8	12
120	Synthesis, size and magnetic properties of controllable MnFe2O4 nanoparticles with versatile surface functionalities. Dalton Transactions, 2014, 43, 9885.	1.6	48
121	Fabrication of noncovalently functionalized brick-like β-cyclodextrins/graphene composite dispersions with favorable stability. RSC Advances, 2014, 4, 2813-2819.	1.7	14
122	Composites of small Ag clusters confined in the channels of well-ordered mesoporous anatase TiO2 and their excellent solar-light-driven photocatalytic performance. Nano Research, 2014, 7, 731-742.	5.8	102
123	Facile Synthesis of Porous Zn <sub>2</sub> Ti <sub>3</sub> O <sub>8</sub> Nanorods for Photocatalytic Overall Water Splitting. ChemCatChem, 2014, 6, 2258-2262.	1.8	30
124	Porous Cobalt Titanate Nanorod: A New Candidate for Visible Lightâ€Driven Photocatalytic Water Oxidation. ChemCatChem, 2014, 6, 265-270.	1.8	81
125	Ordered Mesoporous Black TiO <sub>2</sub> as Highly Efficient Hydrogen Evolution Photocatalyst. Journal of the American Chemical Society, 2014, 136, 9280-9283.	6.6	878
126	Preparation and magnetic performance of the magnetic fluid stabilized by bi-surfactant. Journal of Magnetism and Magnetic Materials, 2013, 332, 151-156.	1.0	21

#	Article	IF	CITATIONS
127	Novel heterogeneous CdS nanoparticles/NiTiO3 nanorods with enhanced visible-light-driven photocatalytic activity. RSC Advances, 2013, 3, 18305.	1.7	56
128	A novel phase-mixed MgTiO3–MgTi2O5 heterogeneous nanorod for high efficiency photocatalytic hydrogen production. Chemical Communications, 2013, 49, 8510.	2.2	62
129	Facile synthesis and shape control of Fe3O4 nanocrystals with good dispersion and stabilization. CrystEngComm, 2013, 15, 3366.	1.3	19
130	Morphology-controlled synthesis of Ag3PO4 nano/microcrystals and their antibacterial properties. Materials Research Bulletin, 2013, 48, 3043-3048.	2.7	51
131	Confinement Effect on Ag Clusters in the Channels of Wellâ€Ordered Mesoporous TiO <sub>2</sub> and their Enhanced Photocatalytic Performance. ChemCatChem, 2013, 5, 1354-1358.	1.8	13
132	Formation and down/up conversion luminescence of Ln3+doped NaY(MoO4)2microcrystals. Dalton Transactions, 2013, 42, 3366-3372.	1.6	31
133	Freeâ€Standing Ultrathin Cobalt Nanosheets Synthesized by Means of In Situ Reduction and Interfaceâ€Directed Assembly and Their Magnetic Properties. ChemPlusChem, 2013, 78, 481-485.	1.3	6
134	Enhanced photoelectric conversion efficiency of dye-sensitized solar cells by the incorporation of dual-mode luminescent NaYF4:Yb3+/Er3+. Dalton Transactions, 2013, 42, 7971.	1.6	47
135	A New Layered Photocathode with Porous NiO Nanosheets: An Effective Candidate for pâ€Type Dye‣ensitized Solar Cells. Chemistry - an Asian Journal, 2013, 8, 3085-3090.	1.7	28
136	High Thermally Stable Mesoporous WO <sub>3</sub> /TiO <sub>2</sub> Heterojunction as a High-Efficient Simulated Solar-Light Photocatalyst. Advanced Porous Materials, 2013, 1, 262-270.	0.3	3
137	Synthesis, luminescence, and photocatalytic activity of KLa <sub>2</sub> Ti <sub>3</sub> O <sub>9.5</sub> :Er <sup>3+</sup> nanocrystals for water decomposition to hydrogen. Journal of Materials Research, 2012, 27, 2925-2929.	1.2	2
138	Room temperature solution synthesis of hierarchical bow-like Cu2O with high visible light driven photocatalytic activity. RSC Advances, 2012, 2, 2875.	1.7	38
139	Anatase TiO2 pillar–nanoparticle composite fabricated by layer-by-layer assembly for high-efficiency dye-sensitized solar cells. Dalton Transactions, 2012, 41, 12683.	1.6	14
140	Facile preparation of porous NiTiO3 nanorods with enhanced visible-light-driven photocatalytic performance. Journal of Materials Chemistry, 2012, 22, 16471.	6.7	176
141	Fabrication of a 3D Hierarchical Flower‣ike MgO Microsphere and Its Application as Heterogeneous Catalyst. European Journal of Inorganic Chemistry, 2012, 2012, 954-960.	1.0	27
142	Photodegradation of organic contamination in wastewaters by bonding TiO2/single-walled carbon nanotube composites with enhanced photocatalytic activity. Chemosphere, 2010, 81, 555-561.	4.2	117
143	Hierarchical anatase TiO2 porous nanopillars with high crystallinity and controlled length: an effective candidate for dye-sensitized solar-cells. Physical Chemistry Chemical Physics, 2010, 12, 9205.	1.3	33
144	The sandwich structure electrodes based on wire-like TiO2–β-cyclodextrin–SWCNT composite for dye-sensitized solar cells. Journal of Photochemistry and Photobiology A: Chemistry, 2009, 207, 306-310.	2.0	3

#	Article	IF	CITATIONS
145	Mesoporous TiO <sub>2</sub> /α-Fe <sub>2</sub> O <sub>3</sub> : Bifunctional Composites for Effective Elimination of Arsenite Contamination through Simultaneous Photocatalytic Oxidation and Adsorption. Journal of Physical Chemistry C, 2008, 112, 19584-19589.	1.5	107